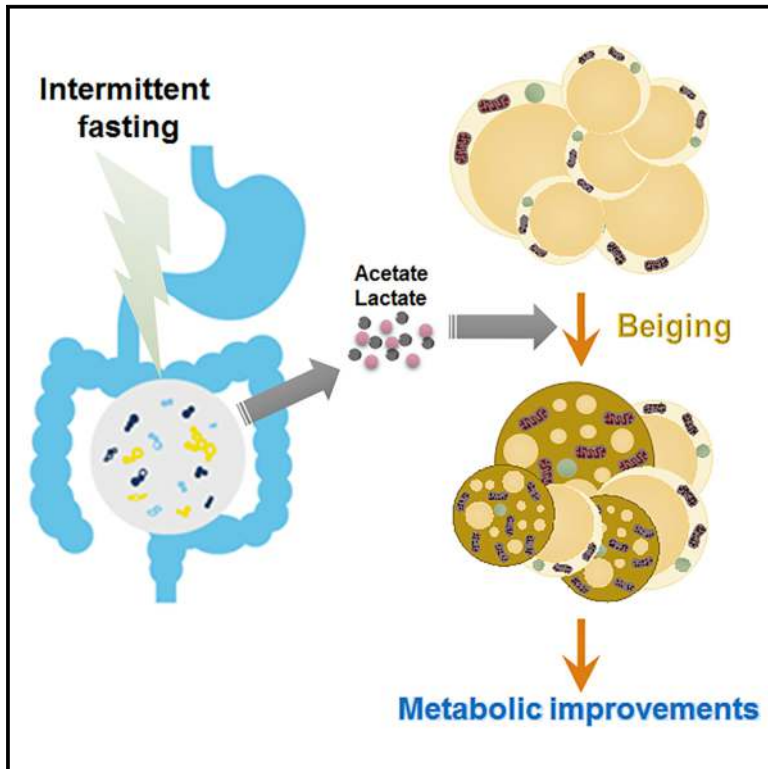


Cell Metabolism

Intermittent Fasting Promotes White Adipose Browning and Decreases Obesity by Shaping the Gut Microbiota

Graphical Abstract



Authors

Guolin Li, Cen Xie, Siyu Lu, ...,
Oksana Gavrilova,
Andrew D. Patterson,
Frank J. Gonzalez

Correspondence

hnsdgl@hunnu.edu.cn (G.L.),
gonzalef@mail.nih.gov (F.J.G.)

In Brief

White adipose beiging is a promising therapy for obesity and related metabolic diseases. Here, Li, Xie and colleagues find that an EODF regimen can selectively induce the beiging of white adipose tissue and subsequently ameliorate metabolic disorders in mice. Gut microbiota orchestrate the effects of EODF on beiging and metabolic improvement.

Highlights

- EODF is a novel strategy for beige adipose development
- EODF selectively induces WAT beiging by reshaping gut microbiota
- EODF reverses high-fat-diet-induced obesity and associated metabolic disorders
- The microbiota-fat axis orchestrates EODF-induced metabolic improvement



Intermittent Fasting Promotes White Adipose Browning and Decreases Obesity by Shaping the Gut Microbiota

Guolin Li,^{1,2,3,7,*} Cen Xie,^{1,7} Siyu Lu,² Robert G. Nichols,⁴ Yuan Tian,⁴ Licen Li,² Daxeshkumar Patel,¹ Yinyan Ma,⁵ Chad N. Brouck,¹ Tingting Yan,¹ Kristopher W. Krausz,¹ Rong Xiang,⁶ Oksana Gavrilova,⁵ Andrew D. Patterson,⁴ and Frank J. Gonzalez^{1,8,*}

¹Laboratory of Metabolism, Center for Cancer Research, National Cancer Institute, National Institutes of Health, Bethesda, MD 20892, USA

²The Key Laboratory of Protein Chemistry and Developmental Biology of Ministry of Education, College of Life Sciences, Hunan Normal University, Changsha, Hunan 410081, China

³The National & Local Joint Engineering Laboratory of Animal Peptide Drug Development, College of Life Sciences, Hunan Normal University, Changsha, Hunan 410081, China

⁴Department of Molecular Toxicology, The Pennsylvania State University, University Park, PA 16802, USA

⁵Mouse Metabolism Core Laboratory, National Institute of Diabetes and Digestive and Kidney Diseases, National Institutes of Health, Bethesda, MD 20892, USA

⁶The State Key Laboratory of Medical Genetics & School of Life Sciences, Central South University, Changsha, Hunan 41001, China

⁷These authors contributed equally

⁸Lead Contact

*Correspondence: hnsdlgl@hunnu.edu.cn (G.L.), gonzalef@mail.nih.gov (F.J.G.)

<http://dx.doi.org/10.1016/j.cmet.2017.08.019>

SUMMARY

While activation of beige thermogenesis is a promising approach for treatment of obesity-associated diseases, there are currently no known pharmacological means of inducing beiging in humans. Intermittent fasting is an effective and natural strategy for weight control, but the mechanism for its efficacy is poorly understood. Here, we show that an every-other-day fasting (EODF) regimen selectively stimulates beige fat development within white adipose tissue and dramatically ameliorates obesity, insulin resistance, and hepatic steatosis. EODF treatment results in a shift in the gut microbiota composition leading to elevation of the fermentation products acetate and lactate and to the selective upregulation of monocarboxylate transporter 1 expression in beige cells. Microbiota-depleted mice are resistance to EODF-induced beiging, while transplantation of the microbiota from EODF-treated mice to microbiota-depleted mice activates beiging and improves metabolic homeostasis. These findings provide a new gut-microbiota-driven mechanism for activating adipose tissue browning and treating metabolic diseases.

INTRODUCTION

Obesity and related metabolic disorders are growing health challenges for Western countries; they mainly result from an imbalance between energy intake and energy expenditure (Hill et al.,

2012; Hossain et al., 2007; Spiegelman and Flier, 2001). Emerging evidence suggests that non-shivering thermogenesis can re-establish energy balance and therefore counter the effects of elevated energy intake (Cannon and Nedergaard, 2011). This process is mediated primarily by the thermogenic activity of uncoupling protein 1 (UCP1), mainly in brown and beige fat cells (Harms and Seale, 2013; Kajimura et al., 2015). In this context, activating brown adipose tissue (BAT) or browning of white adipose tissue (WAT) could be a promising therapy for obesity and related metabolic diseases. Given current thinking that adult humans do not have active BAT (Kajimura et al., 2015; Nedergaard and Cannon, 2014), conversion of white fat to beige fat rather than BAT activation would hold more therapeutic potential. While many browning strategies have been described, mainly in rodent models, only a very limited number of them have so far supported selective browning of WAT (Bonet et al., 2013; Wu et al., 2013). Thus, the therapeutic potential associated with these approaches in a clinical setting is not yet clear.

Recently, intermittent fasting was demonstrated to optimize energy metabolism and promote health (Fontana and Partridge, 2015; Longo and Mattson, 2014). However, the mechanism for these benefits is unclear. Notably, one study found that time-restricted feeding can counteract obesity without reducing energy intake (Hatori et al., 2012). Although perturbation of circadian rhythm was considered as a significant contributor to the increased energy expenditure (Hatori et al., 2012), the possibility exists that white adipose browning would be a more direct mechanism. Therefore, in the current study, mice were placed on an every-other-day fasting (EODF) regimen to explore its effect on white adipose beiging and metabolic disorders. Evidence suggests that EODF selectively activates beige fat thermogenesis and ameliorates obesity-related metabolic diseases, probably via a microbiota-beige fat axis.

RESULTS

EODF Increases Energy Expenditure through Non-shivering Thermogenesis

To determine the adaptive metabolic changes in energy homeostasis induced by intermittent fasting, the effect of 15-cycle EODF on body weight was first analyzed in mice fed a chow diet. When compared with the ad libitum (AL) group, EODF did not affect cumulative food intake (Figure 1A), but reduced body mass gain (Figure 1B), indicative of lower metabolic efficiency and/or higher energy expenditure in EODF mice. To determine the fate of additional energy unaccounted for by body mass gain, the masses of various body depots were analyzed. EODF significantly reduced fat mass—more specifically, visceral epididymal WAT; however, it did not change lean mass and even increased the BAT mass (Figure 1C). These data indicate that EODF treatment might promote adaptive non-shivering thermogenesis and the burning of fat. The circadian core body temperature measured rectally in EODF mice was higher than in the AL group (Figure 1D), as was total energy expenditure (Figures 1E and S1), which suggests that the additional energy intake in EODF mice is released as heat. To determine the primary fuel utilized during this process, whole-body respiratory exchange ratios (RER) were assayed in one cycle of EODF. On the first day (the “fasted” day) of the RER assay, the RER of EODF mice was significantly lower than that of the AL mice, and nearly equal to 0.7 (Figures 1F and S1B), indicating that lipid utilization was a major energy fuel. Although on the second day (the “fed” day), when all mice were feeding, the EODF mice had higher RER, their average RER in a whole EODF cycle was relatively lower than that of their AL counterparts (Figures 1F and S1B). These results indicate that increased utilization of lipid, rather than carbohydrate, is responsible for the increased energy expenditure in EODF mice. Therefore, the EODF treatment appears to favor fat burning.

EODF Selectively Induces Beiging of Inguinal WAT, but Not Activation of BAT

Non-shivering thermogenesis is mainly mediated by activating brown and/or beige adipocytes (Harms and Seale, 2013; Kajimura et al., 2015). Although the above data indicate a mild mass increase in the interscapular BAT in EODF mice (Figure 1C), *Ucp1* expression was significantly suppressed (Figure S2A), and other thermogenic genes, including peroxisome proliferator-activated receptor gamma coactivator 1-alpha (*Pgc1a*) and type II iodothyronine deiodinase (*Dio2*), were not upregulated in either the fed or fasted states of mice treated with EODF (Figures S2B and S2C). The mechanism by which EODF induces higher energy expenditure might differ from that of cold exposure; cold exposure is closely tied to β -AR signaling (Cypess et al., 2015; Mund and Frishman, 2013), while fasting is known to suppress norepinephrine turnover (Knehans and Romsos, 1983) and norepinephrine-induced thermogenesis in BAT (Hayashi and Nagasaka, 1983). In line with these data, EODF did not affect expression of the β_3 -adrenergic receptor (*Adrb3*) mRNA in BAT in the fasted state and suppressed it in the fed state (Figure S2D).

Intriguingly, and in contrast, EODF induced an obvious browning in subcutaneous (inguinal) WAT, as indicated by tissue color

(Figure 1G) and UCP1 expression (Figures 1H and 1I). Histological analysis of inguinal WAT in EODF mice also clearly revealed a significant increase in multilobular adipocytes (Figure 1I), a typical characteristic of beige adipocytes. Although the fold change of *Ucp1* mRNA in the fasted state was relatively lower than in the fed state, the browning phenotype was still pronounced (Figure S3). To determine the washout period for the EODF effect, the 15-cycle EODF-treated mice were placed back on AL feeding. The elevated *Ucp1* mRNA levels in inguinal WAT were significantly diminished on the 7th day after returning to AL feeding and fell to normal levels on the 15th day (Figure S4A). However, the effect of EODF on suppressing weight gain was sustained, as the body weight gain was still significantly lower than the AL group on the 15th day (Figure S4B).

To examine the chronological relationship between WAT beiging and increased energy expenditure induced by EODF, the mice were exposed to short-term EODF. Following 3 cycles of EODF treatment, evident beiging in inguinal WAT was observed as indicated by a striking increase in *Ucp1* mRNA expression (Figure S5A), while body weight and energy expenditure were not obviously changed (Figures S5B–S5D). These results suggest that the effects of EODF on energy expenditure and weight loss are subsequent to its effect on WAT beiging.

The discrepancy of activation between brown and beige cells after EODF conditioning might be due to restricted β -AR-independent thermogenesis in subcutaneous WAT (Ye et al., 2013). The present data suggest that the EODF-induced browning could be independent of β -AR signaling, as EODF treatment significantly downregulated expression of *Adrb3* in both BAT and inguinal WAT under the fed state, and the trend was the same in fasted BAT and WAT (Figures S2D and S3). To further exclude the role of β -AR signaling, mice were acclimatized to thermoneutrality (30°C) for 1 day and then treated with either AL or EODF over the entire period at 30°C. The EODF at 30°C still reduced body weight and fat mass and induced pronounced inguinal WAT beiging, as indicated by increased expression of *Ucp1* mRNA, UCP1 protein, other beige-fat-thermogenic-associated markers, and evident beige morphology (Figures 2A–2E).

EODF-Induced WAT Beiging is Independent of FGF21 Signaling

In addition to β -AR signaling, FGF21 is another classical signaling hormone known to regulate WAT browning (Dutchak et al., 2012; Harms and Seale, 2013) and the adaptive fasting response (Inagaki et al., 2007). However, its expression or its correspondent receptor or obligate co-receptor expression levels in WAT were not altered after the EODF regimen (Figure S3). Liver-derived FGF21 is the most important contributor to circulating FGF21 levels, and PPAR α is a key regulator of hepatic FGF21 (Markan et al., 2014; Montagner et al., 2016). In addition, PPAR α is known to mediate acute fasting-induced upregulation of both hepatic *Fgf21* mRNA and circulating FGF21 protein levels (Montagner et al., 2016). Therefore, *Ppara*^{+/+} and *Ppara*^{-/-} mice were used to examine the role of hepatic FGF21 in the beiging phenotype induced by the EODF regimen. Contrary to an acute fasting model, EODF in wild-type *Ppara*^{+/+} mice was associated with a modest decrease, not increase, in FGF21 expression (Figures 2F and 2G). *Ppara*^{-/-} mice on AL had lower basal *Fgf21* mRNA and circulating FGF21 protein

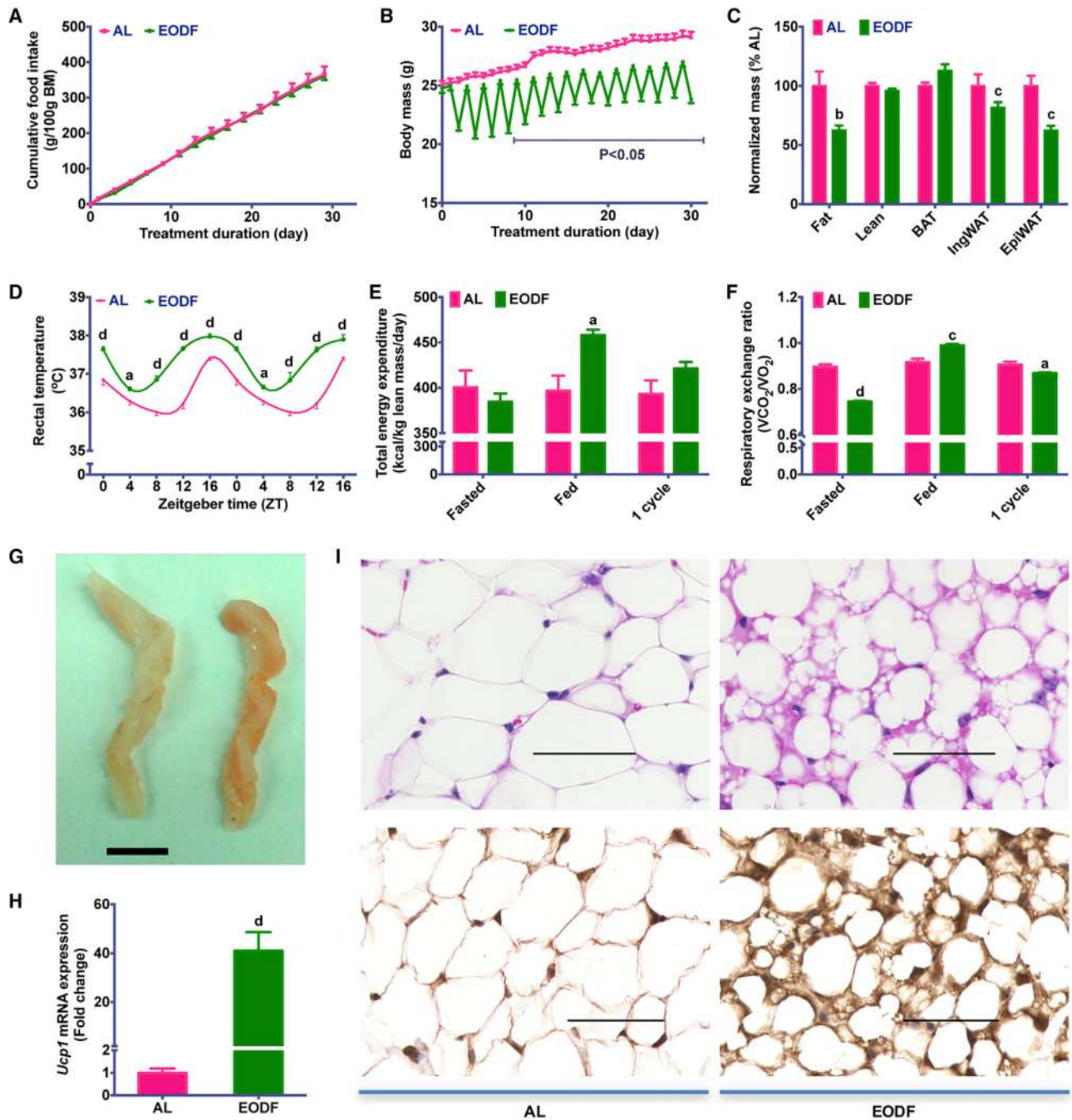


Figure 1. EODF Treatment Increases Energy Expenditure through WAT Beiging

(A) Cumulative food intake; $n = 14$ – 16 mice/group.

(B) Body weight; $n = 14$ – 16 mice/group.

(C) Normalized mass of body depots; $n = 7$ – 8 mice/group.

(D) Circadian rectal temperature on fed day; $n = 14$ – 16 mice/group.

(E and F) Daily total energy expenditure (E) and respiratory exchange ratio (F) during one cycle of EODF. On day 1 (“fasted”), the EODF mice were fasted while the AL mice were fed a chow diet. On day 2 (“fed”), both groups had ad libitum access to chow. Data marked as “1 cycle” show the average value of the 2 days (“fasted” plus “fed”). $n = 4$ mice/group.

(G) Representative image for inguinal WAT of AL (left) and EODF (right) mice. Scale bar: 5 mm.

(H) *Ucp1* mRNA expression in inguinal WAT in the fed state; $n = 7$ – 8 mice/group.

(I) Representative H&E (upper) and UCP1 (lower) staining of inguinal WAT sections. Scale bar: 50 μ m.

Data are presented as mean \pm SEM. Different lowercase letters indicate different statistical significance by two-tailed unpaired t test: a, $p < 0.05$; b, $p < 0.01$; c, $p < 0.005$; and d, $p < 0.001$ versus AL.

See also [Figures S1–S5](#).

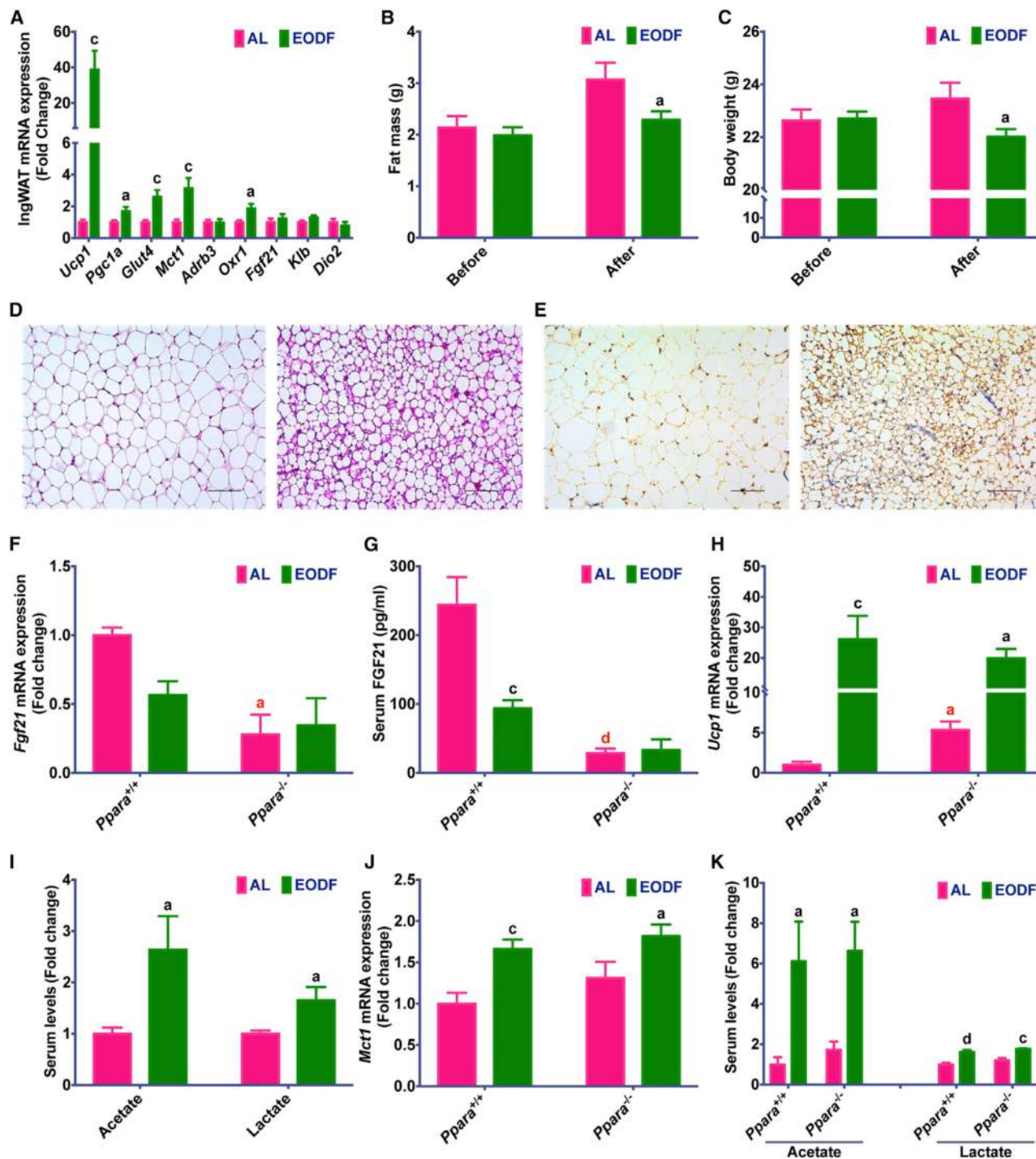


Figure 2. EODF Induces Inguinal WAT Beiging Independent of β -AR and FGF21 Signaling

(A) mRNA expression of thermogenic genes in inguinal WAT of mice under 30°C in the fed state; n = 10 mice/group.

(B) Body weight of mice before and after EODF treatment at 30°C; n = 10 mice/group.

(C) Fat mass of mice before and after EODF treatment at 30°C; n = 10 mice/group.

(D) Representative H&E staining of inguinal WAT sections from EODF (at 30°C) mice (right) and AL mice (left). Scale bar: 100 μm.

(E) Representative UCP1 immunohistochemical staining of inguinal WAT sections from EODF (at 30°C) mice (right) and AL mice (left). Scale bar: 100 μm.

(F and G) Liver *Fgf21* mRNA expression (F) and serum FGF21 levels (G) in *Ppara* wild-type (*Ppara*^{+/+}) and *Ppara*-null (*Ppara*^{-/-}) mice with or without EODF treatment in the fed state; n = 5 mice/group.

(H) mRNA expression of *Ucp1* in inguinal WAT of *Ppara*^{+/+} and *Ppara*^{-/-} mice with or without EODF treatment in the fed state; n = 5 mice/group.

(I) Serum acetate and lactate levels of mice at 30°C; n = 10 mice/group.

(legend continued on next page)

levels (Figures 2F and 2G). As expected, the EODF regimen in *Ppara*^{-/-} mice had no impact on either hepatic *Fgf21* mRNA expression or circulating FGF21 levels (Figures 2F and 2G). EODF did, however, result in a corresponding increase in inguinal WAT *Ucp1* mRNA when compared to *Ppara*^{-/-} AL animals, indicating a comparable beiging phenotype (Figure 2H); this increase was independent of changes in FGF21. Interestingly, WAT from *Ppara*^{-/-} AL mice also exhibited elevated basal *Ucp1* expression when compared to *Ppara*^{+/+} mice (Figure 2H). This suggests that loss of PPAR α signaling promotes a modest increase in beiging in the absence of EODF. Taken together, these data indicate that EODF-induced inguinal WAT beiging does not appear to require FGF21.

Gut Microbiota Orchestrates EODF-Induced WAT Beiging

Recently, correlative evidence revealed a metabolic interaction between the gut microbial communities and the host, and gut bacteria have an important role in the regulation of brown and beige adipose tissues (Chevalier et al., 2015; Holmes et al., 2012; Mestdagh et al., 2012; Nicholson et al., 2012; Rooks and Garrett, 2016; Ziętak et al., 2016). Previous studies revealed that fasting and feeding rhythms significantly alter the gut microbiota (Secor and Carey, 2016; Thaiss et al., 2014) and that major changes in microbiota composition can directly promote WAT beiging (Chevalier et al., 2015). Therefore, it is reasonable to speculate that EODF might induce beiging by altering gut microbiota composition. To test this hypothesis, cecum microbiota communities were profiled by 16S rRNA gene amplicon sequencing. EODF increased the length of the small intestine (Figure 3A) and caused clear alterations in the microbiota content, as indicated by the generalized UniFrac distances (Figure 3B). Hierarchical clustering of individual species confirmed an effect of EODF on the gut microbiome (Figure 3C). According to a previous study (Chevalier et al., 2015), Firmicutes and Bacteroidetes are the most abundant phyla identified in healthy mice; these were present in both EODF and AL groups. However, EODF significantly altered their relative abundance (Figure 3D). Moreover, significant differences were observed in Operational Taxonomic Unit (OTU) abundance at the phylum level in Firmicutes, Bacteroidetes, Actinobacteria, and Tenericutes (Figure 3E). The EODF regimen increased the OTU abundance of Firmicutes while decreasing most other phyla (Figure 3E). Notably, the ratio of Firmicutes:Bacteroidetes increased from 3.4 in AL mice to 8.9 in EODF mice. Intriguingly, similar shifts in the ratio of Firmicutes:Bacteroidetes in mice were reported to be associated with increased glucose uptake in inguinal WAT, but not in interscapular BAT (Chevalier et al., 2015). These data are consistent with the present results that EODF selectively induces beiging of inguinal WAT.

To investigate whether the EODF-induced microbial shift directly contributes to WAT beiging, microbiota from EODF and AL mice—referred as EODF microbiota and AL microbiota,

respectively—were transplanted to microbiota-depleted mice. Transplantation of EODF microbiota significantly upregulated inguinal WAT *Ucp1* mRNA and increased small intestine length when compared to the mice transplanted with AL microbiota (Figures 3A and 3F). Notably, both the intestine length and *Ucp1* mRNA expression in mice transplanted with AL microbiota also increased compared to those of AL mice (Figures 3A and 3F), which is consistent with a previous report that microbiota depletion promotes WAT beiging (Suárez-Zamorano et al., 2015). To explore whether gut microbiota were necessary for EODF-induced beiging, EODF was performed on the microbiota-depleted mice. Indeed, EODF activated beiging only in control mice, but not in microbiota-depleted mice, although the microbiota depletion itself also induced WAT beiging (Figure S6A). Accordingly, the beneficial effects of EODF on several indices of metabolic function were also decreased when the gut microbiota were depleted (Figures S6B–S6G). Therefore, these findings suggest that the effects of EODF on inguinal WAT beiging might be mediated by the gut microbiota.

To further determine the potential mechanism by which gut microbiota influence EODF-induced beiging, ¹H NMR-based metabolomics was carried out on cecal contents obtained from long-term and short-term EODF-treated mice. In order to maximize the discrimination between AL and EODF mice, pairwise orthogonal projection to latent structure-discriminant analysis (OPLS-DA) was performed on normalized NMR data obtained from the cecal contents. Many metabolites changed after EODF treatment, including acetate, lactate, formate, bile acids, propionate, succinate, cytidine monophosphate (CMP), and xanthine, with noted lower levels of trimethylamine (TMA), uracil, and some amino acids, including branch chain amino acids (BCAAs), glycine, tyrosine, and phenylalanine (Figures 4A and 4B). Among these molecules, both acetate and lactate were increased after both long-term and short-term EODF (Figures 4C and 4D). Consistently, EODF treatment also elevated serum acetate and lactate levels (Figures 4C and 4D). Shotgun metagenomics sequencing analysis also showed that EODF upregulated the pathway of “pyruvate fermentation to acetate and lactate by *Lactobacillus reuteri*” and “Pyruvate fermentation to acetate and lactate by unclassified bacteria” (Figure S7). Intriguingly, recent studies indicate that both acetate and lactate are beiging inducers (Hanatani et al., 2016; Kim et al., 2017; Sahuri-Arisoylu et al., 2016). In addition, both BAT and WAT express proton-linked monocarboxylate transporter 1 (MCT1) encoded by *Mct1*, which drives acetate and lactate transport across the plasma membrane of adipocytes (den Besten et al., 2013; Iwanaga et al., 2009). Given recent evidence that the expression of *Mct1* is controlled by physiological stimuli of beiging (Carrière et al., 2014; De Matteis et al., 2013), the selective upregulation of *Mct1* was noted in inguinal WAT, but not in the BAT of either long-term or short-term EODF-treated mice (Figures 4E–4G). The induction of *Mct1*, together with changes in serum acetate and lactate levels, was abolished in microbiota-depleted mice

(J) mRNA expression of *Mct1* in inguinal WAT of *Ppara*^{+/+} and *Ppara*^{-/-} mice with or without EODF treatment in the fed state; n = 5 mice/group.

(K) Serum acetate and lactate levels of *Ppara*^{+/+} and *Ppara*^{-/-} mice with or without EODF treatment; n = 5 mice/group.

Data are presented as mean \pm SEM. Different lowercase letters indicate statistical significance by two-tailed unpaired t test: a, p < 0.05; c, p < 0.005; and d, p < 0.001. Black letters show the effects of EODF (EODF versus AL within the same strain), and red letters show the effects of *Ppara*-null (*Ppara*^{-/-} versus *Ppara*^{+/+} mice within the same treatment). SCFAs, short-chain fatty acids.

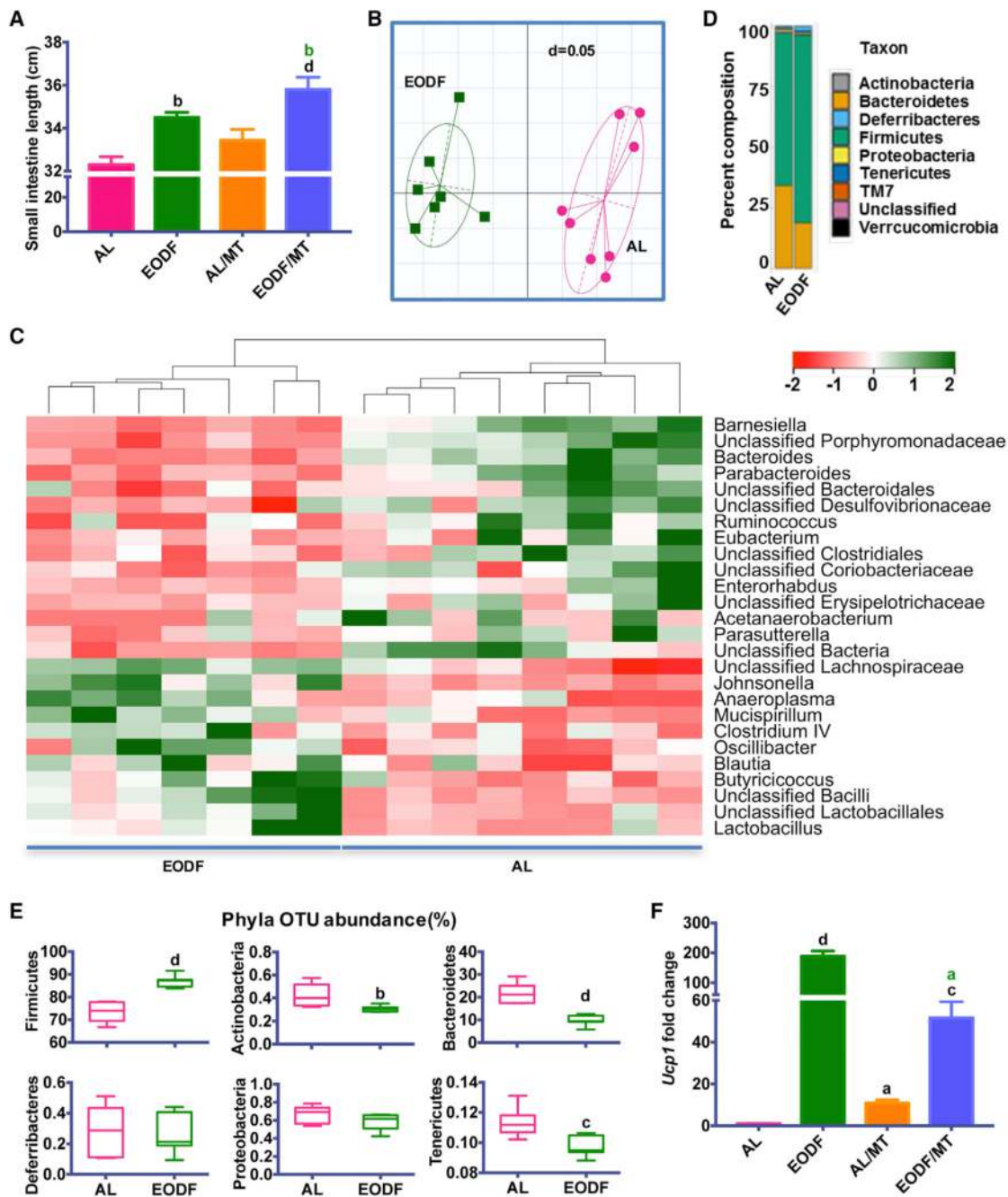


Figure 3. Gut Microbiota Mediates EODF-Induced WAT Beiging

(A) Length of small intestine of AL mice, EODF mice, mice transplanted with AL microbiota (AL/MT), and mice transplanted with EODF microbiota (EODF/MT); $n = 8$ mice/group.

(B) UniFrac distances of AL and EODF mice; $n = 7$ –8 mice/group.

(C) Z scores for genera between AL and EODF mice; $n = 7$ –8 mice/group.

(D) Hierarchical clustering diagram comparing ceca of AL and EODF mice; $n = 7$ –8 mice/group.

(E) Representative Phyla Operational Taxonomic Unit (OTU) abundance (%) of ceca of AL and EODF mice; $n = 7$ –8 mice/group.

(F) *Ucp1* mRNA expression in inguinal WAT in the fed state; $n = 8$ mice/group.

Data are presented as mean \pm SEM. Different lowercase letters indicate different statistical significance by two-tailed unpaired t test (E) or one-way ANOVA with Bonferroni posttest (A and F): a, $p < 0.05$; b, $p < 0.01$; c, $p < 0.005$; and d, $p < 0.001$. Black letters are versus AL, and green letters are versus AL/MT.

See also Figure S6.

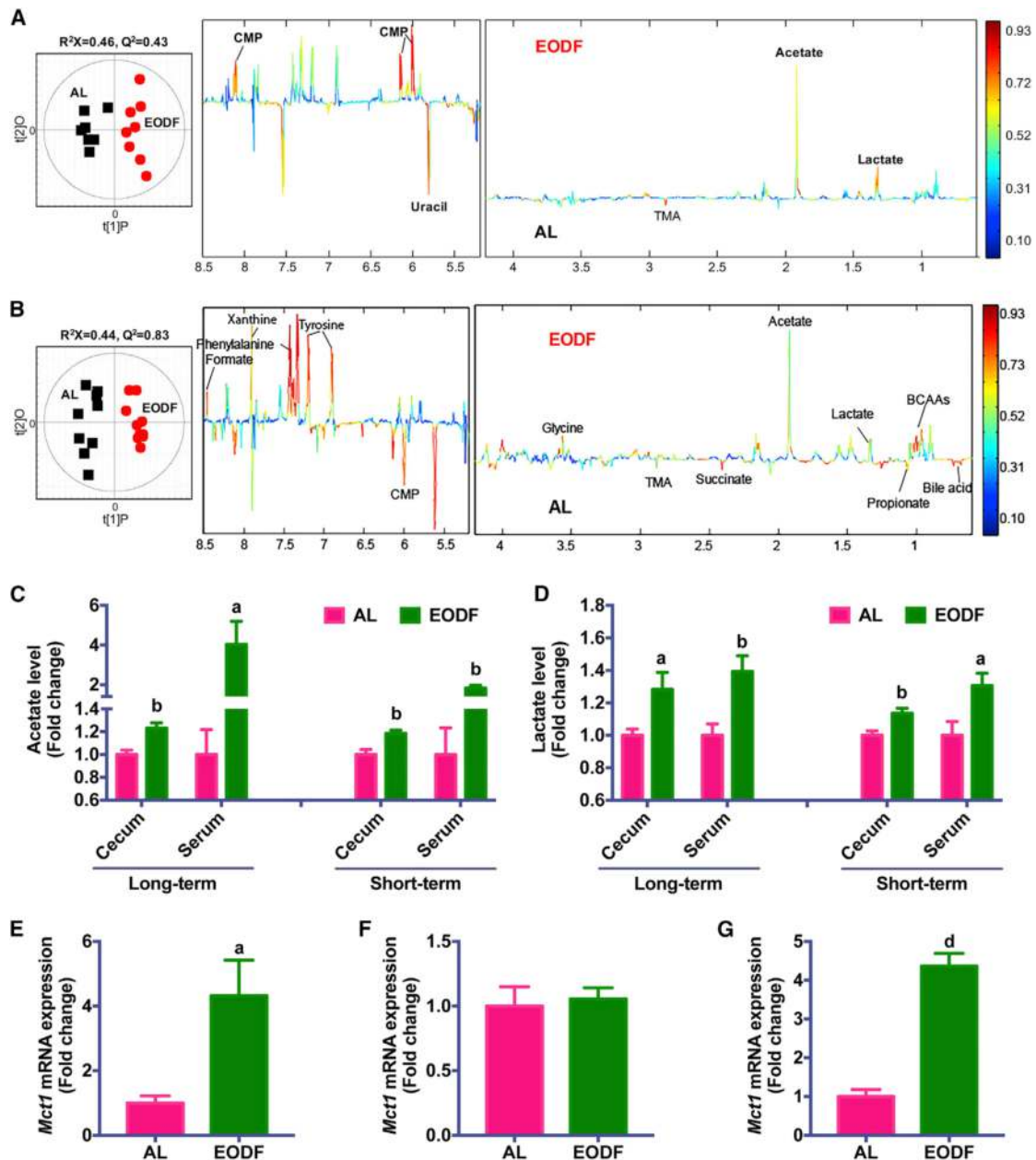


Figure 4. Microbiota Metabolites Underlie the Mechanism of EODF-Induced Beiging

(A) Orthogonal projection to latent structure-discriminant analysis (OPLS-DA) scores (left) and correlation-coefficient-coded loadings plots for the models (right) from NMR spectra of cecal content aqueous extracts from mice after long-term EODF treatment; $n = 7-8$ mice/group.

(B) OPLS-DA scores (left) and correlation-coefficient-coded loadings plots for the models (right) from NMR spectra of cecal content aqueous extracts from mice after short-term EODF treatment; $n = 10$ mice/group.

(C and D) Cecum and serum acetate (C) and lactate (D) levels from mice after long-term and short-term EODF treatment; $n = 7-10$ mice/group.

(E and F) mRNA expression of *Mct1* in inguinal WAT (E) and BAT (F) from mice after long-term EODF treatment in the fed state; $n = 7-8$ mice/group.

(G) mRNA expression of *Mct1* in inguinal WAT from mice after short-term EODF treatment in the fed state; $n = 10$ mice/group.

Data are presented as mean \pm SEM. Different lowercase letters indicate statistical significance by two-tailed unpaired t test: a, $p < 0.05$; b, $p < 0.01$; and d, $p < 0.001$ versus AL.

See also Figure S7.

and restored in mice transplanted with EODF microbiota (Figure S6H). Taken together, these data revealed that EODF primarily alters the gut microbiota composition to promote the generation of acetate and lactate and, subsequently, to induce inguinal WAT beiging. Moreover, neither the thermoneutral condition nor the deficiency of PPAR α abolished the effect of EODF on promoting the increase of *Mct1* mRNA expression in inguinal WAT and of serum acetate and lactate levels (Figures 2A and 2I–2K), supporting the conclusion that the effects of EODF are independent of β -AR or PPAR α signaling, but associated with gut-microbiota-derived metabolites.

EODF Ameliorates Metabolic Syndrome in Obese Mice

Given that activation of beige cells can suppress obesity and metabolic disease (Harms and Seale, 2013), the effect of an EODF regimen on diet-induced obesity (DIO) mice was explored. Mice were fed a HFD for 3 months and then subjected to either the AL or EODF regimens (15 cycles). EODF mice displayed pronounced weight loss, in contrast to their AL counterparts, without any difference in their cumulative food intake (Figures 5A and 5B). EODF mice had dramatically lower body weights that correlated with the number of EODF cycles (Figure 5C). Consistent with the above data that EODF upregulated *Glut4* in lean mice (Figure S3), EODF also increased inguinal WAT *Glut4* mRNA expression and thus improved insulin sensitivity in DIO mice (Figures 5D and 5E). Moreover, liver steatosis and injury markers in EODF mice were obviously ameliorated (Figure 5F). EODF resulted in a more significant reduction of inguinal fat mass than of epididymal fat mass (Figure 5G). Thus, EODF could differentially impact visceral and subcutaneous fat depots.

BAT and inguinal WAT gene expression in DIO mice, in response to the EODF regimen, displayed a similar trend to that found in lean mice. *Ucp1* and *Pgc1a* mRNA upregulation occurred in the inguinal WAT, but not in the BAT, of EODF mice (Figures 5D and 5H). The mRNAs encoding β -AR and FGF21 signaling-related receptors were not altered (Figure 5D). These results hint that EODF-induced WAT beiging might be involved in the beneficial effects of EODF on obesity-associated metabolic syndrome in DIO mice.

Gut Microbiota Contribute to the Beneficial Effects of EODF on DIO Mice

Gut microbiota play a critical role in energy metabolism and lipid homeostasis, and germfree or microbiota-depleted rodents have decreased susceptibility to diet-induced obesity and metabolic syndrome (Bäckhed et al., 2007; Rabot et al., 2010; Suárez-Zamorano et al., 2015). Based on the above findings, EODF treatment could alter the microbiota compositions and prevent HFD-induced obesity and metabolic disorders. To further clarify the role of gut microbiota in mediating the beneficial effects of EODF regimen on metabolic diseases, the effect of EODF in control and microbiota-depleted DIO mice was compared. EODF treatment significantly reduced obesity and hepatic steatosis and improved insulin sensitivity in control mice, but not in microbiota-depleted mice (Figures 6A–6G), indicating that the effects of EODF depend on gut microbiota. To examine whether gut microbiota are sufficient to replicate the effects of EODF, microbiota-depleted DIO mice were transplanted with AL microbiota and EODF microbiota, respectively. Compared with the AL

microbiota-transplanted group, EODF microbiota transplantation did mimic all the beneficial effects of EODF treatment on metabolic dysfunctions (Figures 6A–6H). Moreover, in line with the above results from lean mice, EODF-induced inguinal WAT beiging occurred in control DIO mice, but not in their microbiota-depleted counterparts (Figure 7A). EODF microbiota transplantation to DIO mice promoted inguinal WAT *Ucp1* mRNA and UCP1 protein expression, an increase in multilobular adipocytes, and enhanced energy expenditure with lower RER (Figures 7B–7F). Accordingly, the EODF-induced elevated levels of serum acetate, serum lactate, and inguinal WAT *Mct1* mRNA were abolished by microbiota depletion but restored by EODF microbiota transplantation (Figures 7A, 7B, 7G, and 7H). These findings underscore an important role for gut microbiota in the beneficial effects of EODF on WAT beiging and the subsequent improvements in metabolic diseases.

DISCUSSION

In this study, EODF was found to substantially induce beiging in subcutaneous inguinal WAT. Although many agents and treatments were reported to induce browning (Bonet et al., 2013; Jiang et al., 2015; Wu et al., 2013), it is unclear how these approaches can translate to clinically relevant therapies for human metabolic disease (Nedergaard and Cannon, 2014). In contrast, intermittent fasting (including EODF) has been practiced in humans, especially in certain religious groups (Patterson et al., 2015), for centuries and has been proven to benefit body composition and health (Eshghinia and Mohammadzadeh, 2013; López-Bueno et al., 2014; Patterson et al., 2015). To date, few studies have examined whether this regimen can induce WAT beiging. Most fasting-related studies have focused on BAT, but not subcutaneous WAT, revealing that fasting suppresses both BAT UCP1 expression and norepinephrine-induced thermogenesis (Desautels and Dulos, 1988; Hayashi and Nagasaka, 1983; Sivit et al., 1999). In support of these findings, results from the current study identified lower *Ucp1* and *Adrb3* mRNA expression in the BAT of EODF mice. However, this is not the case in subcutaneous WAT, as shown in the current study; UCP1 expression was dramatically upregulated after intermittent fasting.

A striking finding from this study is that EODF selectively activates beige, but not brown, adipocytes. Cold acclimation was originally found to increase the number of brown adipocytes in the parametrical fat pad in mice (Young et al., 1984). Since that finding, more than a hundred alternate treatments have been shown to activate both brown and beige adipose (Bonet et al., 2013; Wu et al., 2013). Brown adipocyte activation by cold exposure or by β -AR agonists is clinically non-feasible, and adult human BAT is largely composed of beige-like adipocytes (Shinoda et al., 2015). Therefore, understanding the underlying mechanisms driving the selective beiging of certain white depots during EODF could reveal new therapeutic targets for the prevention and treatment of metabolic disease, which might provide alternative pharmaceutical options for those who cannot sustain intermittent fasting for long periods of time.

Implicit in the present findings is that gut microbiota mediates the mechanism of EODF-induced beiging. Despite the many proposed mechanisms for adipose browning, β -AR signaling is

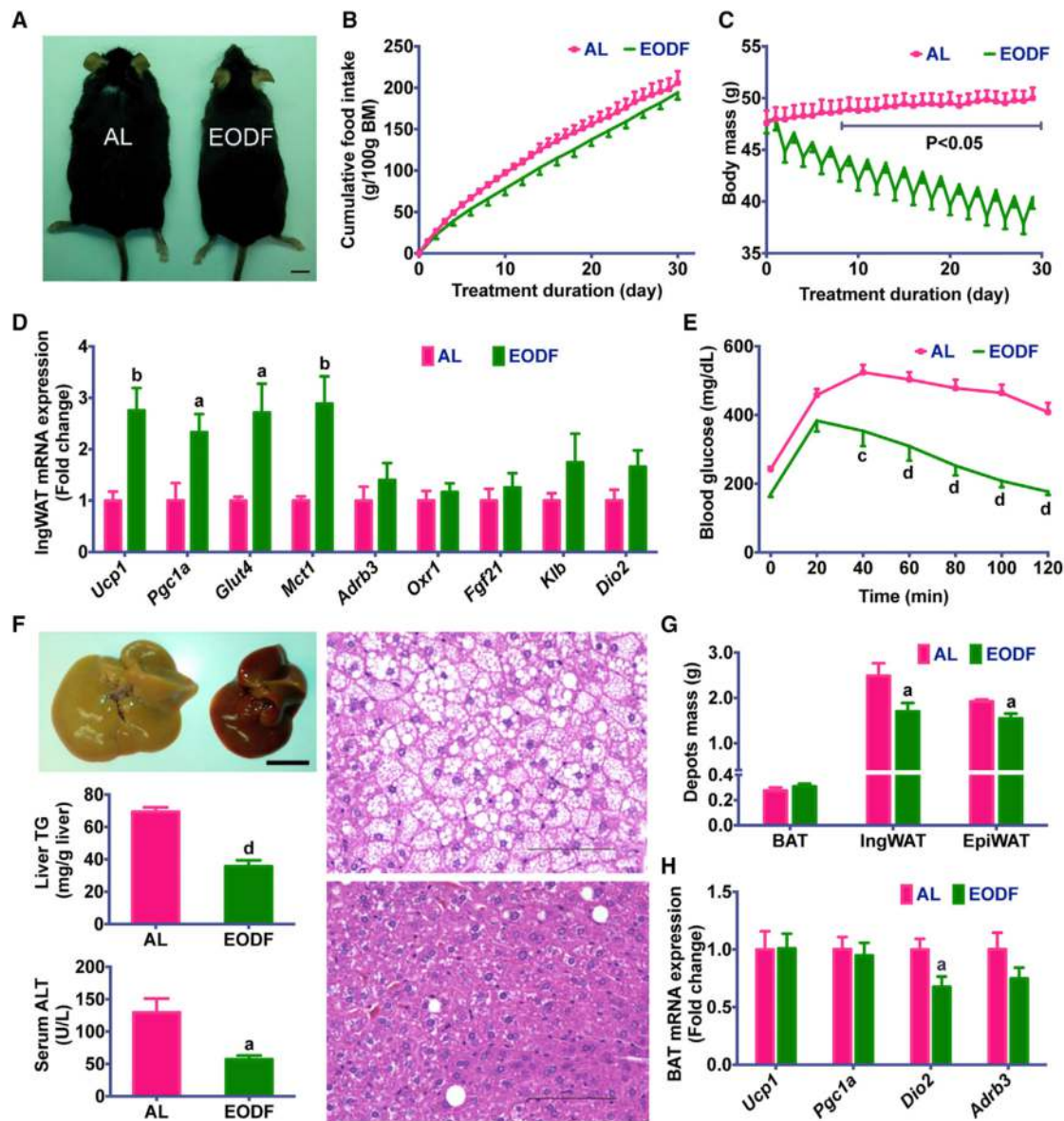


Figure 5. EODF Ameliorates Metabolic Dysfunction in DIO Mice

(A) Representative AL and EODF mouse. Scale bar: 5 mm.

(B) Cumulative food intake.

(C) Body weight.

(D) mRNA expression of thermogenic genes in inguinal WAT in the fed state.

(E) Glucose tolerance test.

(F) Liver function. Upper left, representative image of livers from AL mouse (left) and EODF mouse (right). Scale bar: 5 mm. Middle left, liver triglycerides; lower left, serum ALT. Right, representative H&E staining of liver sections from AL (upper) and EODF (lower) mice. Scale bar: 100 μ m.

(G) Fat depot mass.

(H) mRNA expression of thermogenic genes in interscapular BAT in the fed state.

Data are presented as mean \pm SEM; $n = 6$ mice/group. Different lowercase letters indicate different statistical significance by two-tailed unpaired t test: a, $p < 0.05$; b, $p < 0.01$; c, $p < 0.005$; and d, $p < 0.001$ versus AL.

still the prototypical pathway and currently the most intensely studied (Robidoux et al., 2004; Susulic et al., 1995). While BAT activation mainly depends on β -AR signaling, the browning of subcutaneous WAT under certain conditions might be independent of β -AR signaling (Ye et al., 2013). Consistently, EODF only activated subcutaneous WAT, but not BAT, and the mechanism

for EODF-induced being might be independent of β -AR signaling. Recent studies have shown that interactions between the host and gut microbiota affect many aspects of energy metabolism (Takeda, 2016). The microbiome influences cold-induced adipose being and modulates metabolic syndrome and other diseases (Chevalier et al., 2015; Holmes et al., 2012;

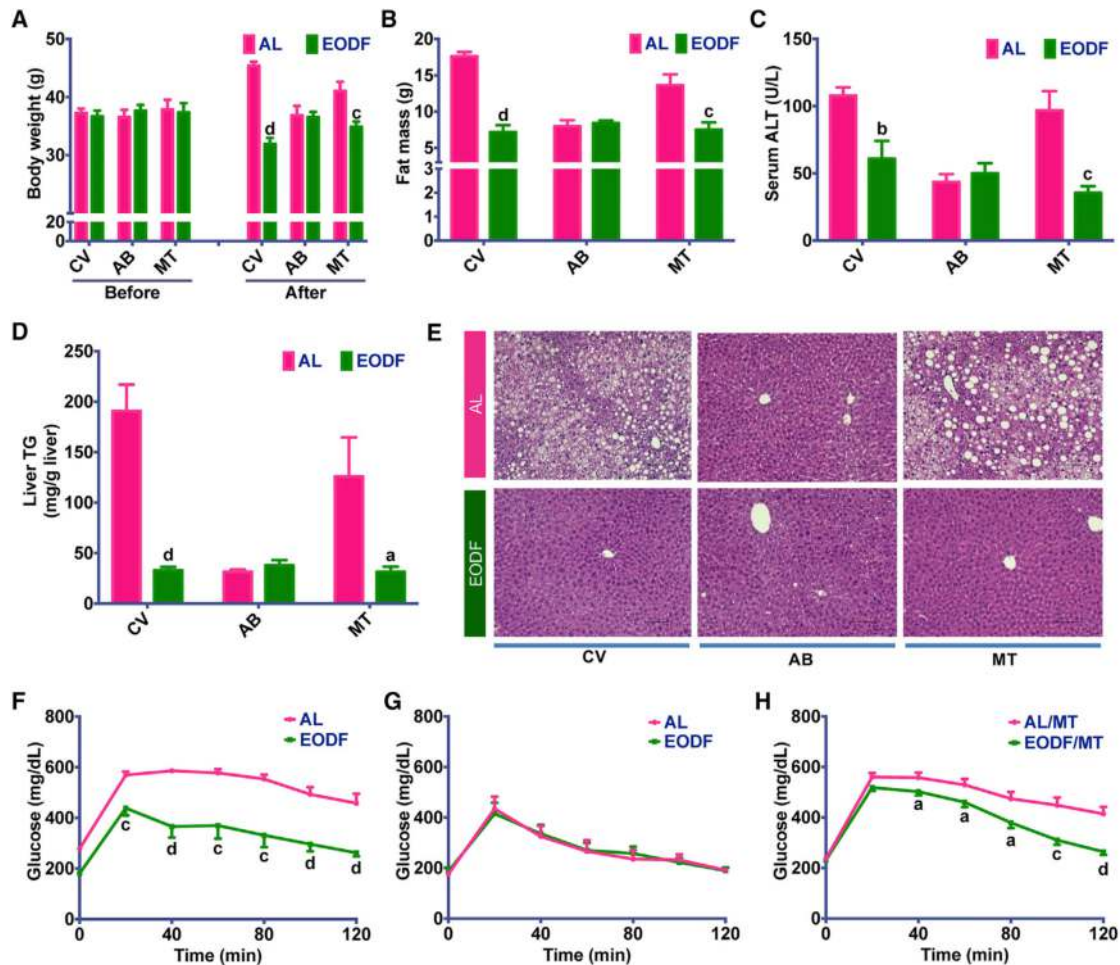


Figure 6. Gut Microbiota Mediates the Effects of EODF on Metabolic Syndrome in DIO Mice

(A) Body weight. Before EODF or microbiota transplantation (MT) treatment, all mice were given access to control vehicle (CV) water or water supplemented with an antibiotics cocktail (AB) for 4 weeks. $n = 6-8$ mice/group.

(B) Fat mass; $n = 6-8$ mice/group.

(C) Serum ALT; $n = 6-8$ mice/group.

(D) Liver triglycerides; $n = 6-8$ mice/group.

(E) Representative H&E staining of liver sections. Scale bar: 100 μm .

(F and G) Glucose tolerance test in CV-treated (F) or AB-treated (G) mice; $n = 6$ mice/group.

(H) Glucose tolerance test in MT mice receiving microbiota from AL (AL/MT) or EODF donors (EODF/MT); $n = 8$ mice/group.

Data are presented as mean \pm SEM. Different lowercase letters indicate statistical significance by two-tailed unpaired t test: a, $p < 0.05$; b, $p < 0.01$; c, $p < 0.005$; and d, $p < 0.001$. Black letters show the effects of EODF or EODF/TM (EODF versus AL, or EODF/MT versus AL/MT with access to the same water).

Suárez-Zamorano et al., 2015). Intriguingly, the alteration in gut microbe composition resulting from EODF is similar to the changes found in a previous report supporting a causal role for microbiota in WAT beiging (Chevalier et al., 2015). Transplantation of EODF microbiota to microbiota-depleted mice promoted beiging of inguinal WAT, while EODF cannot induce beiging in the absence of gut microbiota; this suggests that gut flora is required for EODF-induced WAT beiging. It should be noted that microbiota-depleted mice were established by antibiotics treatment in the current study. We cannot exclude the possibility that some metabolic changes may have been due to the absorbed fraction of antibiotics.

Another important finding from the present study is that EODF causes dramatic weight loss and attenuates metabolic dysfunc-

tion in mice by directly activating beige cells through shaping the gut microbiota. A recent report revealed that restriction of feeding periods prevents HFD-induced weight gain and metabolic syndrome without reducing total caloric intake; these effects were attributed to alterations in circadian rhythms (Hatori et al., 2012). The present work revealed that EODF treatment also does not affect cumulative food intake, thus demonstrating that weight loss may result from increased energy expenditure. Conversely, EODF treatment did not appear to affect circadian rhythms, as rectal temperature profiles and metabolic curves in EODF animals paralleled those of the AL control groups. Therefore, the mechanism for EODF-induced weight loss does not appear to be the result of circadian perturbation. On the other hand, the prominent function of activated beige cells is to

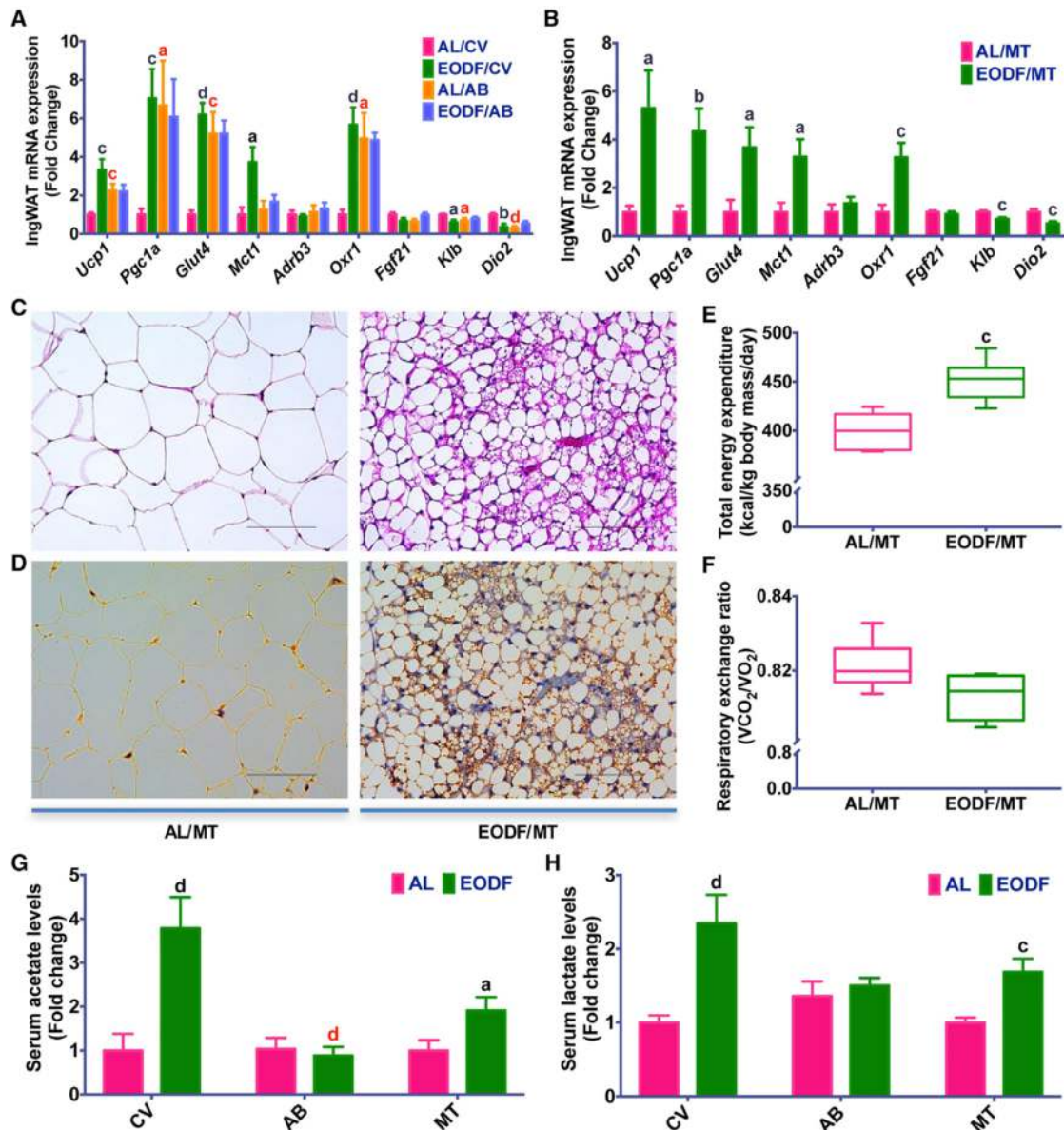


Figure 7. Gut Microbiota Mediates the Effects of EODF on Inguinal WAT Beiging in DIO Mice

(A and B) mRNA expression of thermogenic genes in inguinal WAT in the fed state. All mice were given access to control vehicle (CV) water or water supplemented with an antibiotics cocktail (AB) for 4 weeks and were then treated with AL or EODF (A) or microbiota transplantation (MT, B). $n = 6-8$ mice/group.

(C) Representative H&E staining of inguinal WAT from mice transplanted with EODF microbiota (EODF/MT, right) and AL microbiota (AL/MT, left). Scale bar: 100 μ m.

(D) Representative UCP1 immunohistochemical staining of inguinal WAT sections from EODF/MT (right) and AL/MT (left) mice. Scale bar: 100 μ m.

(E and F) Daily total energy expenditure (E) and respiratory exchange ratio (F) of AL/MT and EODF/MT mice; $n = 6$ mice/group.

(G and H) Serum acetate (G) and lactate (H) of DIO mice after EODF or MT treatment. Before EODF or MT treatment, all mice were given access to CV or AB water for 4 weeks. $n = 6-8$ mice/group.

Data are presented as mean \pm SEM. Different lowercase letters indicate statistical significance by two-way ANOVA with Sidak multiple comparisons (A) or two-tailed unpaired t test (B and E-H): a, $p < 0.05$; c, $p < 0.005$; and d, $p < 0.001$. Black letters show the effects of EODF or EODF/MT (EODF versus AL or EODF/MT versus AL/MT drunk with the same water), and red letters show the effects of microbiota depletion (AB versus CV within the same feeding regimen).

promote thermogenesis and suppresses obesity (Ishibashi and Seale, 2010; Shabalina et al., 2013; Wu et al., 2012). The present study reveals pronounced beiging of inguinal WAT, and the mechanism for this EODF-induced improvement in metabolic syndrome could be, at least in part, attributed to increased ther-

mogenesis as a result of WAT beiging. Moreover, consistent with an important role for gut microbiota in inducing beiging, EODF microbiota transplantation can reproduce the effects of an EODF regimen, and EODF fails to further improve obesity-related diseases in microbiota-depleted mice.

In summary, the present work uncovered novel perspectives on beige-fat development in the inguinal WAT. EODF was shown to selectively activate beige fat, probably by re-shaping the gut microbiota, which led to increases in the beige stimuli acetate and lactate. EODF also dramatically ameliorated metabolic syndrome in a mouse model of obesity. This alternative beige fat activation by EODF offers new insights into the microbiota-beige fat axis and provides a novel therapeutic approach for the treatment of obesity-related metabolic disorders.

STAR★METHODS

Detailed methods are provided in the online version of this paper and include the following:

- **KEY RESOURCES TABLE**
- **CONTACT FOR REAGENT AND RESOURCE SHARING**
- **EXPERIMENTAL MODEL DETAILS**
 - Animals
- **METHOD DETAILS**
 - EODF Treatment
 - Gut Microbiota Transplantation
 - Gut Microbiota Profiling
 - Cecal NMR Metabolomics
 - Gut Bacteria Metagenomic Assay
 - Serum Lactate and Acetate Determination
 - Body Composition and Indirect Calorimetry
 - Glucose Tolerance Test
 - Lipid Analysis
 - Serum Aminotransferase Assay
 - Serum FGF21 Assay
 - Real-Time PCR
 - H&E and Immunohistochemistry Staining
- **QUANTIFICATION AND STATISTICAL ANALYSIS**
 - Statistical Analysis
- **DATA AND SOFTWARE AVAILABILITY**
 - MATLAB Script and Data

SUPPLEMENTAL INFORMATION

Supplemental Information includes seven figures and one table and can be found with this article online at <http://dx.doi.org/10.1016/j.cmet.2017.08.019>.

AUTHOR CONTRIBUTIONS

G.L., C.X., S.L., R.G.N., Y.T., C.N.B., D.P., Y.M., T.Y., L.L., K.W.K., and O.G. performed the research and analyzed the data. G.L., C.X., R.X., O.G., A.D.P., and F.J.G. designed and supervised the research. G.L., C.X., and F.J.G. wrote the manuscript.

ACKNOWLEDGMENTS

We thank Linda G. Byrd for technical assistance with the mouse studies. We thank Dongxue Sun, Jiang Yue, Jie Zhao, Lei Chen, Qiao Wang, Qiong Wang, Qiu Wang, Weiwei Liu, Xiaoxia Gao, Xianqiong Gong, Yoshinori Takizawa, Youbo Zhang, and Yuhong Luo for help with the mouse studies. This work was funded by the National Cancer Institute Intramural Research Program (ZIA BC005562), the National Institutes of Environmental Health Sciences (ES022186, to A.D.P.), the National Natural Science Funds of China (31271257, 9164910027, and 81403007), the Science and Technology Project of Hunan Province (2013FJ2001), and the Cooperative Innovation Center of Engineering and New Products for Developmental Biology of Hunan Province

(20134486). G.L. was supported by a fellowship from the Chinese Scholarship Council (201406725005). The funding sponsors had no role in the design; in the collection, analysis, and interpretation of data; in the writing of the manuscript; or in the decision to submit the manuscript for publication.

Received: December 20, 2016

Revised: May 10, 2017

Accepted: August 17, 2017

Published: September 14, 2017; corrected online: October 24, 2017

REFERENCES

- Abreu-Vieira, G., Xiao, C., Gavrilova, O., and Reitman, M.L. (2015). Integration of body temperature into the analysis of energy expenditure in the mouse. *Mol. Metab.* *4*, 461–470.
- Abubucker, S., Segata, N., Goll, J., Schubert, A.M., Izard, J., Cantarel, B.L., Rodriguez-Mueller, B., Zucker, J., Thiagarajan, M., Henrissat, B., et al. (2012). Metabolic reconstruction for metagenomic data and its application to the human microbiome. *PLoS Comput. Biol.* *8*, e1002358.
- Bäckhed, F., Manchester, J.K., Semenkovich, C.F., and Gordon, J.I. (2007). Mechanisms underlying the resistance to diet-induced obesity in germ-free mice. *Proc. Natl. Acad. Sci. USA* *104*, 979–984.
- Bonet, M.L., Oliver, P., and Palou, A. (2013). Pharmacological and nutritional agents promoting browning of white adipose tissue. *Biochim. Biophys. Acta* *1831*, 969–985.
- Buchfink, B., Xie, C., and Huson, D.H. (2015). Fast and sensitive protein alignment using DIAMOND. *Nat. Methods* *12*, 59–60.
- Cannon, B., and Nedergaard, J. (2011). Nonshivering thermogenesis and its adequate measurement in metabolic studies. *J. Exp. Biol.* *214*, 242–253.
- Carrière, A., Jeanson, Y., Berger-Müller, S., André, M., Chenouard, V., Arnaud, E., Barreau, C., Walther, R., Galinier, A., Wdziekonski, B., et al. (2014). Browning of white adipose cells by intermediate metabolites: an adaptive mechanism to alleviate redox pressure. *Diabetes* *63*, 3253–3265.
- Chen, J., Bittinger, K., Charlson, E.S., Hoffmann, C., Lewis, J., Wu, G.D., Collman, R.G., Bushman, F.D., and Li, H. (2012). Associating microbiome composition with environmental covariates using generalized UniFrac distances. *Bioinformatics* *28*, 2106–2113.
- Chevalier, C., Stojanović, O., Colin, D.J., Suarez-Zamorano, N., Tarallo, V., Veyrat-Durebex, C., Rigo, D., Fabbiano, S., Stevanović, A., Hagemann, S., et al. (2015). Gut microbiota orchestrates energy homeostasis during cold. *Cell* *163*, 1360–1374.
- Cypess, A.M., Weiner, L.S., Roberts-Toler, C., Franquet Elía, E., Kessler, S.H., Kahn, P.A., English, J., Chatman, K., Trauger, S.A., Doria, A., and Kolodny, G.M. (2015). Activation of human brown adipose tissue by a β 3-adrenergic receptor agonist. *Cell Metab.* *21*, 33–38.
- De Matteis, R., Lucertini, F., Guescini, M., Polidori, E., Zeppa, S., Stocchi, V., Cinti, S., and Cuppini, R. (2013). Exercise as a new physiological stimulus for brown adipose tissue activity. *Nutr. Metab. Cardiovasc. Dis.* *23*, 582–590.
- den Besten, G., van Eunen, K., Groen, A.K., Venema, K., Reijngoud, D.J., and Bakker, B.M. (2013). The role of short-chain fatty acids in the interplay between diet, gut microbiota, and host energy metabolism. *J. Lipid Res.* *54*, 2325–2340.
- Desautels, M., and Dullos, R.A. (1988). Effects of repeated cycles of fasting-re-feeding on brown adipose tissue composition in mice. *Am. J. Physiol.* *255*, E120–E128.
- Dutchak, P.A., Katafuchi, T., Bookout, A.L., Choi, J.H., Yu, R.T., Mangelsdorf, D.J., and Kliewer, S.A. (2012). Fibroblast growth factor-21 regulates PPAR γ activity and the antidiabetic actions of thiazolidinediones. *Cell* *148*, 556–567.
- Eshghinia, S., and Mohammadzadeh, F. (2013). The effects of modified alternate-day fasting diet on weight loss and CAD risk factors in overweight and obese women. *J. Diabetes Metab. Disord.* *12*, 4.
- Fontana, L., and Partridge, L. (2015). Promoting health and longevity through diet: from model organisms to humans. *Cell* *161*, 106–118.

- Hanatani, S., Motoshima, H., Takaki, Y., Kawasaki, S., Igata, M., Matsumura, T., Kondo, T., Senokuchi, T., Ishii, N., Kawashima, J., et al. (2016). Acetate alters expression of genes involved in beige adipogenesis in 3T3-L1 cells and obese KK-Ay mice. *J. Clin. Biochem. Nutr.* *59*, 207–214.
- Harms, M., and Seale, P. (2013). Brown and beige fat: development, function and therapeutic potential. *Nat. Med.* *19*, 1252–1263.
- Hatori, M., Vollmers, C., Zarrinpar, A., DiTacchio, L., Bushong, E.A., Gill, S., Leblanc, M., Chaix, A., Joens, M., Fitzpatrick, J.A., et al. (2012). Time-restricted feeding without reducing caloric intake prevents metabolic diseases in mice fed a high-fat diet. *Cell Metab.* *15*, 848–860.
- Hayashi, M., and Nagasaka, T. (1983). Suppression of norepinephrine-induced thermogenesis in brown adipose tissue by fasting. *Am. J. Physiol.* *245*, E582–E586.
- Hill, J.O., Wyatt, H.R., and Peters, J.C. (2012). Energy balance and obesity. *Circulation* *126*, 126–132.
- Holmes, E., Li, J.V., Marchesi, J.R., and Nicholson, J.K. (2012). Gut microbiota composition and activity in relation to host metabolic phenotype and disease risk. *Cell Metab.* *16*, 559–564.
- Hossain, P., Kowar, B., and El Nahas, M. (2007). Obesity and diabetes in the developing world—a growing challenge. *N. Engl. J. Med.* *356*, 213–215.
- Inagaki, T., Dutchak, P., Zhao, G., Ding, X., Gautron, L., Parameswara, V., Li, Y., Goetz, R., Mohammadi, M., Esser, V., et al. (2007). Endocrine regulation of the fasting response by PPAR α -mediated induction of fibroblast growth factor 21. *Cell Metab.* *5*, 415–425.
- Ishibashi, J., and Seale, P. (2010). Medicine. Beige can be slimming. *Science* *328*, 1113–1114.
- Iwanaga, T., Kuchiiwa, T., and Saito, M. (2009). Histochemical demonstration of monocarboxylate transporters in mouse brown adipose tissue. *Biomed. Res.* *30*, 217–225.
- Jiang, C., Xie, C., Lv, Y., Li, J., Krausz, K.W., Shi, J., Brocker, C.N., Desai, D., Amin, S.G., Bisson, W.H., et al. (2015). Intestine-selective farnesoid X receptor inhibition improves obesity-related metabolic dysfunction. *Nat. Commun.* *6*, 10166.
- Kajimura, S., Spiegelman, B.M., and Seale, P. (2015). Brown and beige fat: physiological roles beyond heat generation. *Cell Metab.* *22*, 546–559.
- Kim, N., Nam, M., Kang, M.S., Lee, J.O., Lee, Y.W., Hwang, G.S., and Kim, H.S. (2017). Piperine regulates UCP1 through the AMPK pathway by generating intracellular lactate production in muscle cells. *Sci. Rep.* *7*, 41066.
- Knehans, A.W., and Romsos, D.R. (1983). Norepinephrine turnover in obese (ob/ob) mice: effects of age, fasting, and acute cold. *Am. J. Physiol.* *244*, E567–E574.
- Kozich, J.J., Westcott, S.L., Baxter, N.T., Highlander, S.K., and Schloss, P.D. (2013). Development of a dual-index sequencing strategy and curation pipeline for analyzing amplicon sequence data on the MiSeq Illumina sequencing platform. *Appl. Environ. Microbiol.* *79*, 5112–5120.
- Langille, M.G., Zaneveld, J., Caporaso, J.G., McDonald, D., Knights, D., Reyes, J.A., Clemente, J.C., Burkpile, D.E., Vega Thurber, R.L., Knight, R., et al. (2013). Predictive functional profiling of microbial communities using 16S rRNA marker gene sequences. *Nat. Biotechnol.* *31*, 814–821.
- Langmead, B., and Salzberg, S.L. (2012). Fast gapped-read alignment with Bowtie 2. *Nat. Methods* *9*, 357–359.
- Lee, S.S., Pineau, T., Drago, J., Lee, E.J., Owens, J.W., Kroetz, D.L., Fernandez-Salguero, P.M., Westphal, H., and Gonzalez, F.J. (1995). Targeted disruption of the alpha isoform of the peroxisome proliferator-activated receptor gene in mice results in abolishment of the pleiotropic effects of peroxisome proliferators. *Mol. Cell. Biol.* *15*, 3012–3022.
- Longo, V.D., and Mattson, M.P. (2014). Fasting: molecular mechanisms and clinical applications. *Cell Metab.* *19*, 181–192.
- López-Bueno, M., González-Jiménez, E., Navarro-Prado, S., Montero-Alonso, M.A., and Schmidt-RioValle, J. (2014). Influence of age and religious fasting on the body composition of Muslim women living in a westernized context. *Nutr. Hosp.* *31*, 1067–1073.
- Markan, K.R., Naber, M.C., Ameka, M.K., Anderegg, M.D., Mangelsdorf, D.J., Kliewer, S.A., Mohammadi, M., and Potthoff, M.J. (2014). Circulating FGF21 is liver derived and enhances glucose uptake during refeeding and overfeeding. *Diabetes* *63*, 4057–4063.
- Mestdagh, R., Dumas, M.E., Rezzi, S., Kochhar, S., Holmes, E., Claus, S.P., and Nicholson, J.K. (2012). Gut microbiota modulate the metabolism of brown adipose tissue in mice. *J. Proteome Res.* *11*, 620–630.
- Montagner, A., Polizzi, A., Fouché, E., Ducheix, S., Lippi, Y., Lasserre, F., Barquissau, V., Régnier, M., Lukowicz, C., Benhamed, F., et al. (2016). Liver PPAR α is crucial for whole-body fatty acid homeostasis and is protective against NAFLD. *Gut* *65*, 1202–1214.
- Mund, R.A., and Frishman, W.H. (2013). Brown adipose tissue thermogenesis: β 3-adrenoreceptors as a potential target for the treatment of obesity in humans. *Cardiol. Rev.* *21*, 265–269.
- Nedergaard, J., and Cannon, B. (2014). The browning of white adipose tissue: some burning issues. *Cell Metab.* *20*, 396–407.
- Nicholson, J.K., Holmes, E., Kinross, J., Burcellin, R., Gibson, G., Jia, W., and Pettersson, S. (2012). Host-gut microbiota metabolic interactions. *Science* *336*, 1262–1267.
- Patel, D.P., Krausz, K.W., Xie, C., Beyoğlu, D., Gonzalez, F.J., and Idle, J.R. (2017). Metabolic profiling by gas chromatography-mass spectrometry of energy metabolism in high-fat diet-fed obese mice. *PLoS One* *12*, e0177953.
- Patterson, R.E., Laughlin, G.A., LaCroix, A.Z., Hartman, S.J., Natarajan, L., Senger, C.M., Martínez, M.E., Villaseñor, A., Sears, D.D., Marinac, C.R., and Gallo, L.C. (2015). Intermittent fasting and human metabolic health. *J. Acad. Nutr. Diet.* *115*, 1203–1212.
- Rabot, S., Membrez, M., Bruneau, A., Gérard, P., Harach, T., Moser, M., Raymond, F., Mansourian, R., and Chou, C.J. (2010). Germ-free C57BL/6J mice are resistant to high-fat-diet-induced insulin resistance and have altered cholesterol metabolism. *FASEB J.* *24*, 4948–4959.
- Robidoux, J., Martin, T.L., and Collins, S. (2004). Beta-adrenergic receptors and regulation of energy expenditure: a family affair. *Annu. Rev. Pharmacol. Toxicol.* *44*, 297–323.
- Rooks, M.G., and Garrett, W.S. (2016). Gut microbiota, metabolites and host immunity. *Nat. Rev. Immunol.* *16*, 341–352.
- Sahuri-Arisoylu, M., Brody, L.P., Parkinson, J.R., Parkes, H., Navaratnam, N., Miller, A.D., Thomas, E.L., Frost, G., and Bell, J.D. (2016). Reprogramming of hepatic fat accumulation and ‘browning’ of adipose tissue by the short-chain fatty acid acetate. *Int. J. Obes.* *40*, 955–963.
- Secor, S.M., and Carey, H.V. (2016). Integrative physiology of fasting. *Compr. Physiol.* *6*, 773–825.
- Segata, N., Izard, J., Waldron, L., Gevers, D., Miropolsky, L., Garrett, W.S., and Huttenhower, C. (2011). Metagenomic biomarker discovery and explanation. *Genome Biol.* *12*, R60.
- Shabalina, I.G., Petrovic, N., de Jong, J.M., Kalinovich, A.V., Cannon, B., and Nedergaard, J. (2013). UCP1 in brite/beige adipose tissue mitochondria is functionally thermogenic. *Cell Rep.* *5*, 1196–1203.
- Shinoda, K., Luijten, I.H., Hasegawa, Y., Hong, H., Sonne, S.B., Kim, M., Xue, R., Chondronikola, M., Cypess, A.M., Tseng, Y.H., et al. (2015). Genetic and functional characterization of clonally derived adult human brown adipocytes. *Nat. Med.* *21*, 389–394.
- Sivitz, W.I., Fink, B.D., and Donohoue, P.A. (1999). Fasting and leptin modulate adipose and muscle uncoupling protein: divergent effects between messenger ribonucleic acid and protein expression. *Endocrinology* *140*, 1511–1519.
- Spiegelman, B.M., and Flier, J.S. (2001). Obesity and the regulation of energy balance. *Cell* *104*, 531–543.
- Suárez-Zamorano, N., Fabbiano, S., Chevalier, C., Stojanović, O., Colin, D.J., Stevanović, A., Veyrat-Durebex, C., Tarallo, V., Rigo, D., Germain, S., et al. (2015). Microbiota depletion promotes browning of white adipose tissue and reduces obesity. *Nat. Med.* *21*, 1497–1501.
- Susulic, V.S., Frederich, R.C., Lawitts, J., Tozzo, E., Kahn, B.B., Harper, M.E., Himms-Hagen, J., Flier, J.S., and Lowell, B.B. (1995). Targeted disruption of the beta 3-adrenergic receptor gene. *J. Biol. Chem.* *270*, 29483–29492.
- Takeda, K. (2016). Metabolic bridge between microbiota and humans. *Nat. Rev. Immunol.* *16*, 206.

- Thaiss, C.A., Zeevi, D., Levy, M., Zilberman-Schapira, G., Suez, J., Tengeler, A.C., Abramson, L., Katz, M.N., Korem, T., Zmora, N., et al. (2014). Transkingdom control of microbiota diurnal oscillations promotes metabolic homeostasis. *Cell* *159*, 514–529.
- Tian, Y., Zhang, L., Wang, Y., and Tang, H. (2012). Age-related topographical metabolic signatures for the rat gastrointestinal contents. *J. Proteome Res.* *11*, 1397–1411.
- Truong, D.T., Franzosa, E.A., Tickle, T.L., Scholz, M., Weingart, G., Pasolli, E., Tett, A., Huttenhower, C., and Segata, N. (2015). MetaPhlan2 for enhanced metagenomic taxonomic profiling. *Nat. Methods* *12*, 902–903.
- Wu, J., Boström, P., Sparks, L.M., Ye, L., Choi, J.H., Giang, A.H., Khandekar, M., Virtanen, K.A., Nuutila, P., Schaart, G., et al. (2012). Beige adipocytes are a distinct type of thermogenic fat cell in mouse and human. *Cell* *150*, 366–376.
- Wu, J., Cohen, P., and Spiegelman, B.M. (2013). Adaptive thermogenesis in adipocytes: is beige the new brown? *Genes Dev.* *27*, 234–250.
- Ye, L., Wu, J., Cohen, P., Kazak, L., Khandekar, M.J., Jedrychowski, M.P., Zeng, X., Gygi, S.P., and Spiegelman, B.M. (2013). Fat cells directly sense temperature to activate thermogenesis. *Proc. Natl. Acad. Sci. USA* *110*, 12480–12485.
- Young, P., Arch, J.R., and Ashwell, M. (1984). Brown adipose tissue in the parametrial fat pad of the mouse. *FEBS Lett.* *167*, 10–14.
- Ziętak, M., Kovatcheva-Datchary, P., Markiewicz, L.H., Ståhlman, M., Kozak, L.P., and Bäckhed, F. (2016). Altered microbiota contributes to reduced diet-induced obesity upon cold exposure. *Cell Metab.* *23*, 1216–1223.

STAR★METHODS

KEY RESOURCES TABLE

REAGENT or RESOURCE	SOURCE	IDENTIFIER
Antibodies		
rabbit polyclonal anti-UCP1	Abcam	Cat# ab10983; RRID: AB_2241462
Chemicals, Peptides, and Recombinant Proteins		
bacitracin	Sigma-Aldrich	Cat# B0125; CAS: 1405-87-4
gentamycin	Sigma-Aldrich	Cat# G1914; CAS: 1405-41-0
ciprofloxacin	Sigma-Aldrich	Cat# 17850; CAS: 85721-33-1
neomycin	Sigma-Aldrich	Cat# N6386; CAS: 1405-10-3
penicillin	Sigma-Aldrich	Cat# A70909; CAS: 551-16-6
metronidazole	Sigma-Aldrich	Cat# M1547; CAS: 443-48-1
ceftazidime	Sigma-Aldrich	Cat# C3809; CAS: 120618-65-7
streptomycin	Sigma-Aldrich	Cat# 46754; CAS: 3810-74-0
vancomycin	Sigma-Aldrich	Cat# v2002; CAS: 1404-93-9
Normal rabbit IgG	Santa cruz	Cat#SC-2027
Critical Commercial Assays		
ALT assay kit	Catachem Inc	Cat# V165-12
Mouse FGF21 ELISA Kit	R&D Systems	Cat# MF2100
Wako Clinical Diagnostics kits	Wako Life Sciences, Inc	Cat# 994-02891/992-02892; Cat# 990-02991/998-02992; Cat# 464-01601
E.Z.N.A.® Stool DNA Kit	OMEGA bio-tek	Cat# D4015-02
Experimental Models: Organisms/Strains		
Mouse: C57BL/6	Charles River Laboratories	Strain Code: 027
Mouse: Ppara wild-type (Ppara+/+): C57BL/6	(Lee et al., 1995)	N/A
Mouse: Ppara-null (Ppara-/-): C57BL/6	(Lee et al., 1995)	N/A
Oligonucleotides		
Primers for qPCR, see Table S1	This paper	N/A
Software and Algorithms		
GraphPad Prism 7.0	http://www.graphpad.com/	N/A
SIMCA-P+ software 13.0	http://umetrics.com/	N/A
MATLAB	The Mathworks Inc	N/A
MATLAB Script and Data	R script and data for key statistical results	Available upon request to the Lead Contact.
Deposited Data		
16S rRNA sequencing data	SRA	accession number # PRJNA398633

CONTACT FOR REAGENT AND RESOURCE SHARING

Further information and requests for resources and reagents should be directed to and will be fulfilled by the Lead Contact, Frank J. Gonzalez (gonzalef@mail.nih.gov), following an approved Material Transfer Agreement between the National Cancer Institute and the receiving institution.

EXPERIMENTAL MODEL DETAILS

Animals

All mouse studies were approved by the NCI Animal Care and Use Committee and performed in accordance with the Institute of Laboratory Animal Resources guidelines. Six-week-old male C57BL/6N mice were purchased from Charles River Laboratories.

The *Ppara* wild-type (*Ppara*^{+/+}) and conventional *Ppara* null (*Ppara*^{-/-}) mice on a pure C57BL/6N background used in this study were described previously (Lee et al., 1995). Mice were housed in a temperature (22°C)- and light-controlled vivarium with free access to water and standard rodent chow food or high fat diet (HFD) (S3282 from Bio-Serv). All experiments were started with 7- to 8-week-old mice.

METHOD DETAILS

EODF Treatment

Mice were randomly grouped to ad libitum (AL) group and every other day fasting (EODF) group. All mice were co-housed (2 mice per cage) on chow diet or single housed on HFD for 2 weeks prior to study initiation to allow for acclimation to the animal facility and were then placed on chow diet or HFD. Under the chow diet, the AL group mice were allowed unrestricted access to food, while EODF groups were fed with alternating 24 hr periods (15 cycles for long-term study and 3 cycles for short-term study) of free access to food followed by 24 hr fasting. Under the HFD, mice were allowed unrestricted access to HFD for 3 months to induce an obese phenotype then randomly separated into AL and EODF groups and subjected to the AL or EODF feeding regimen (15 cycles). For EODF at thermoneutrality, mice were acclimatized to thermoneutrality (30°C) for 1 day and then treated either AL or EODF over the entire period at thermoneutrality (30°C) condition. Body weight was measured daily. Food intake was calculated daily quantifying the weight of the remaining food. Data were normalized to the body weight of the mice.

Gut Microbiota Transplantation

Microbiota transplantation were done according to a previous study (Chevalier et al., 2015). In brief, fresh antibiotics (1 mg/ml bacitracin, 170 µg/ml gentamycin, 125 µg/ml ciprofloxacin, 100 µg/ml neomycin, 100 U/ml penicillin, 100 µg/ml metronidazole, 100 µg/ml ceftazidime, 50 µg/ml streptomycin and 50 µg/ml vancomycin, Sigma) were added into the drinking water of mice, and changed once a week. After 4 weeks of antibiotics treatment, the antibiotics-containing water was replaced with the regular water. The microbiota-depleted mice were co-housing with AL or EODF donor animals on the fed day and kept in the donors' cages on the fasted day for four days, and then transplanted with AL or EODF microbiota by gavaging with 20 mg fresh feces from donors re-suspended in 400 µL sterile anaerobic PBS. Following transplantation, the mice were co-housed with AL or EODF donor animals on the fed day and kept in the donors' cages on the fasted day for another 10 days. Then, animals were euthanized and tissues collected.

Gut Microbiota Profiling

Bacteria from cecal contents were extracted with the E.Z.N.A stool DNA kit (OMEGA bio-tek) according to the protocol provided. Extracted DNA was measured by Nanodrop and aliquots were taken to provide a final concentration of 20 ng/µl for each DNA sample. PCR analysis was performed on the aliquoted DNA using the V4-V4 primer set. PCR mixtures were initially heated to 94°C for 3 min, followed by 20 cycles of 94°C for 15 s, 55°C for 45 s, and 72°C for 60 s. Reactions were completed at 72°C for 8 min. The PCR products were analyzed by running 5 µL of the product on a 1% agarose gel and found to average of 350 base pairs. PCR products were sent to the Penn State Genomics Core Facility (University Park, PA) for library preparation. Paired end sequencing was performed on the Illumina Miseq platform, and the sequencing results sent back for analysis. 16S rRNA gene amplicon sequence results were analyzed using the MOTHUR platform (Kozich et al., 2013) and aligned to SILVA and Green Genes databases separately. Analysis to the SILVA database provided data for GUnifrac analysis. A phylogenetic tree and Operation Taxonomic Unit (OTU) table were obtained from the Mothur Bayesian classifier (Kozich et al., 2013) and uploaded to R studio for GUnifrac analysis (Chen et al., 2012). After Green Genes alignment, a .biom file was created and uploaded onto the Huttenhower galaxy page. PICRUST analysis was done on the .biom file resulting in a pathway abundance file (Langille et al., 2013). LEfSe (Segata et al., 2011) was used to obtain statistically significant and biologically relevant pathways from pathway abundance file.

Cecal NMR Metabolomics

The cecal content samples for NMR was prepared as previously described (Tian et al., 2012). ¹H NMR spectra were recorded at 298 K on a Bruker Avance III 600 MHz spectrometer equipped with an inverse cryogenic probe (Bruker Biospin, Germany). NMR spectra of all the cecal content samples were acquired for each employing the first increment of NOESY pulse sequence (NOESYPR1D) with the recycle delay (RD) of 2 s and mixing time (t_m) of 100 ms. The 90° pulse length was adjusted to about 10 µs for each sample and 64 transients were collected into 32 k data points for each spectrum with spectral width of 20 ppm. The chemical shift of ¹H NMR spectra were referenced to TSP at δ 0.00. Each bucketed region (0.004 ppm) was then normalized to the total sum of the spectral integrals prior to statistical data analysis. Orthogonal projection to latent structure-discriminant analysis (OPLS-DA) were carried out using the SIMCA-P+ software (Version 13.0, Umetrics, Sweden). Back-transformed loadings from the OPLS-DA models were performed with color-coded correlation coefficient for variables, using an in-house developed script for MATLAB (The Mathworks Inc., Natwick, MA). The metabolites were assigned based on the published data and confirmed with a series of 2D NMR experiments (Tian et al., 2012). The relative contents of lactate at δ 1.33 and acetate at δ 1.92 were calculated against the total sum of the spectral integrals.

Gut Bacteria Metagenomic Assay

Bacteria from cecal contents were extracted with the E.Z.N.A stool DNA kit (OMEGA bio-tek) according to the protocol provided by the manufacturer. Bacterial extracts were measured with nanodrop and raw bacterial isolation samples were transferred to the

Pennsylvania State University Genomics Core Facility for Illumina HiSeq shotgun metagenomic sequencing (150x150 paired end). The TruSeq DNA PCR free kit was used to prepare libraries for metagenomic analysis. The Humann2 (Abubucker et al., 2012) pipeline was used for functional pathway discovery on the samples. This pipeline uses the MetaPIAn 2 (Truong et al., 2015) software to assign taxonomic information to the HiSeq reads being sequenced. Assigned reads were piped into Bowtie2 (Langmead and Salzberg, 2012) which provided functional information to the taxonomic assigned reads with the ChocoPhlAn database. Unassigned reads were piped into DIAMOND which converts the DNA reads into protein sequences and aligns them to a protein database to obtain functional information (Buchfink et al., 2015). Results from DIAMOND and results from Bowtie 2 are piped into the core algorithms of Humann2 which results in a gene families file, a pathway coverage file, and a pathway abundance file. Pathways with coverage below 30% were removed from further analysis. LEfSE (Segata et al., 2011) was used to obtain biological relevance and statistical significance from the functional information.

Serum Lactate and Acetate Determination

Gas chromatography–mass spectrometry (GC–MS) analysis was performed with an Agilent 6890N gas chromatograph coupled to an Agilent 5973 mass-selective detector (Agilent Technologies, Santa, CA). Data processing were conducted with Agilent mass hunter work station software (Agilent Technologies). For lactate, serum was prepared and analyzed as previously described by GC–MS (Patel et al., 2017). For acetate quantification, serum was spiked with 2-butyniic acid (internal standard, 10 μ M) in acetonitrile. The samples were centrifuged at 20,000 g for 10 min at 4°C and the supernatants were dried in a SpeedVac concentrator at room temperature. The residue was dissolved in methanol: H₂O (80:20, v/v, pH 2-3) and injected into the GC–MS.

Body Composition and Indirect Calorimetry

Body fat and lean mass of non-anesthetized live mice were determined using an EchoMRI 3-in-1 mouse scanner (EchoMRI, Houston, TX) following manufacturer's protocol. Indirect calorimetry was performed on mice after 14 cycles of EODF treatment using a 12-chamber Environment Controlled CLAMS (Columbus Instruments, Columbus, OH) with one mouse/chamber as previously described (Abreu-Vieira et al., 2015). After 48-h acclimatization, mice were monitored for 24 h at feeding state and then 20 hr at fast-ing state for recording data. During testing, water was provided ad libitum. Locomotor activity was determined at the same time as energy expenditure was measured using infrared beam interruption.

Glucose Tolerance Test

Mice were fasted for 6 h, and fasted glucose was measured using a Glucometer (Bayer, Pittsburgh, PA) by tail bleeds. Then mice were intraperitoneally injected with 2 g glucose/kg of body weight, and blood glucose was measured at intervals of 20 min for 2 hr.

Lipid Analysis

For analysis of liver lipid content, 20 mg of frozen liver was homogenized by TissueLyser-96 (Shanghai Jingxin Co. Ltd, Shanghai, China) in 400 μ L of 50 mM Tris with 5% Triton X-100, and then the samples were heated to 80–100°C and cooled to room temperature (repeated twice). After centrifugation supernatants were diluted 10-fold and quantified using Wako Clinical Diagnostics kits (Wako USA, Richmond, VA).

Serum Aminotransferase Assay

Serum alanine aminotransferase (ALT) were assessed in a 96-well microplate using a commercial ALT assay kit (Catachem, Bridgeport, CT), and monitored at 340 nm for 10 min with a microplate reader (BioAssay Systems, Harvard, CA).

Serum FGF21 Assay

Serum fibroblast growth factor 21 (FGF21) were assessed in a 96-well microplate using a mouse/rat FGF21 quantikine ELISA kit (R&D Systems), and read at 450 nm with a microplate reader.

Real-Time PCR

Total RNA was extracted from frozen tissues using TRIzol reagent according to the manufacturer's instructions. The purity and concentration of the total RNA were determined by a NanoDrop spectrophotometer (ND-1000, Thermo Fisher). Fifty ng of total RNA was reverse transcribed using cDNA Synthesis SuperMix (Biotool.com). Real-time PCR was carried out in an ABI 7900HT Fast Real-Time PCR System (AB Applied Biosystems, Warrington, UK) with SYBR Green PCR master mix (AB Applied Biosystems) and gene-specific primers. The sequence and GenBank accession number for the forward and reverse primers used to quantify mRNA were listed in the Table S1. The following conditions were used for real-time PCR: 95°C for 10min, then 95°C for 15 s and 60°C for 1 min in 40 cycles. The $2^{-\Delta\Delta CT}$ method was used to analyze the relative changes in gene expression normalized against 18S rRNA or *Gapdh* mRNA expression.

H&E and Immunohistochemistry Staining

All tissues were fixed in 4% paraformaldehyde for 24 hr at room temperature, dehydrated and embedded into paraffin. Then tissues were sectioned into thick slices (4 μ m) and stained with hematoxyline and eosin (H&E). For immunohistochemistry, slides were at first rinsed with 0.05% Triton X-100 in PBS, and non-specific binding sites were blocked using 1% bovine serum albumin (BSA) in PBS

containing 0.05% Tween 20. Epitope retrieval was carried out using autoclave (15 min in citrate buffer, pH 6.0). After cooling to room temperature, the slides were incubated overnight at 4°C with rabbit polyclonal anti-UCP1 primary antibody (ab10983; Abcam) diluted 1:500 in PBS containing 1% BSA. The slides were rinsed in distilled water, followed by treating with HRP-conjugated goat anti-rabbit IgG using the ABC method with a commercially available kit (Vector Laboratories, Burlingame, CA) according to the manufacturer's instruction. Immunovisualization was carried out with 3, 3'-diaminobenzidine (DAB) as substrate (Sigma), and counterstained with hematoxylin. Slide digital images were collected at 10-40 X magnification with a KEYENCE BZ-X710 Fluorescence Microscope (Keyence Inc., Itasca, IL). Images shown are representative results of at least three biological replicates.

QUANTIFICATION AND STATISTICAL ANALYSIS

Statistical Analysis

All results are expressed as means \pm SEM. Computations assumed that all groups were samples from populations with the same scatter. The investigators involved in this study were not completely blinded during sample collection or data analysis in the animal experiments. Outliers were identified by outlier analysis using the ROUT method (Prism 7.0 software, GraphPad Software, San Diego, CA) and excluded from statistical analyses. Significance was determined by (multiple) two-tailed unpaired t test, one-way ANOVA with Bonferroni posttest, or two-way ANOVA with Sidak multiple comparisons using Prism 7.0 software. A P value of < 0.05 was considered significant.

DATA AND SOFTWARE AVAILABILITY

MATLAB Script and Data

The MATLAB script and associated data (which were used to make the back-transformed loading graphs in [Figures 4A and 4B](#)) will be provided upon request to the Lead Contact. The accession number for the sequence reported in this paper is SRA: PRJNA398633.